Unusual Luminescence Spectra and Decay Dynamics in Crystalline Supramolecular $[(A18C6)_4MBr_4][TlBr_4]_2$ (A = Rb, K; M = 3d Element) Complexes

Nicolette S. Fender,[†] Frank R. Fronczek,[‡] Vijay John,[§] Ishenkumba A. Kahwa,*[,†] and Gary L. McPherson[||]

Department of Chemistry, University of the West Indies, Mona, Kingston 7, Jamaica, Department of Chemistry, Louisiana State University, Baton Rouge, Louisiana 70803, and Departments of Chemical Engineering and Chemistry, Tulane University, New Orleans, Louisiana 70118

Received February 16, 1996[⊗]

Luminescence and electronic energy transport characteristics of supramolecular cubic *F*23 $[(A18C6)_4MnBr_4][TlBr_4]_2$ complexes (A = Rb, **1**; A = K, **2**) were studied with the expectation that $MnBr_4^{2-}$ ions would be effective luminescent probes for solid state 18-crown-6 rotation-conformational reorientation motion frequently revealed by NMR methods. Luminescence and excitation spectra of **1** are normal for complexes of $MnBr_4^{2-}$, but complex **2** features an unusual orange emission (due to crystal defects) with $\lambda_{max} \approx 570$ nm which is sensitized by $MnBr_4^{2-}$ ions. Thermal barriers of 8 and 14 kJ mol^{-1} ($T < 210$ K and $T > 240$ K, respectively) for **1** ($MnBr_4^{2-}$ $\lambda_{em} = 511$ nm) and **2** (crystal defect $\lambda_{em} = 610$ nm) are attributed to the energy required to bridge the Stokes shifted $^4T_1(^4G)$ emission of the donor $MnBr_4^{2-}$ ions with the electronic origin of the $^4T_1(^4G)$ state on the acceptor $MnBr_4^{2-}$ during energy migration. That of 26 kJ mol^{-1} ($210 < T < 240$ K) exhibited by **1** is attributed to the activation energy for the 18C6 solid state motion inferable from the single, broad, featureless solid state ^{13}C NMR band of $[(K18C6)_4ZnBr_4][TlBr_4]_2$ (**3**). Crystal data for $[(K18C6)_4MBr_4][TlBr_4]_2$, where M = Mn (Zn): space group *F*23 and $Z = 4$ for both complexes; $a = 20.986(7)$ (20.9682(7)) Å, $V = 9242.8(3)$ (9219.0(3)) Å^3, number of observed data = 672 (668), $R_w = 0.037$ (0.039), $R = 0.062$ (0.036).

Introduction

Metal-rich 18-crown-6 (18C6) complexes featuring the general stoichiometry $[(A18C6)_4MX_4][BX_4]_2 \cdot nH_2O$ crystallize in the cubic *F*23 form.[1−3] Usually, A = a large monovalent cation, such as Rb, Tl, or BaX, B = a trivalent cation, such as Tl or Fe, M = a divalent 3d cation, and X = halide. A recent study of energy transport properties of crystals of $[(A18C6)_4MnCl_4][TlCl_4]_2 \cdot nH_2O$ (A = Rb, Tl) revealed a thermally activated energy migration process on the $[(A18C6)_4MnCl_4]^{2+}$ sublattice which culminates in energy transfer to lattice water traps.[4] However, the temperature dependence of the energy transfer process was not consistent with the behavior of multiphonon processes[5] based on luminescence quenching by water vibrations. Instead, the thermalized luminescence quenching process exhibited an onset temperature of roughly 200 K and a thermal barrier of ca. 50 kJ mol^{-1}. This behavior is remarkably similar to the temperature evolution of the rotation-conformational reorientation motion of 18C6. For example, in a series of cross polarization magic angle spinning ^{13}C NMR studies of numerous solid 18C6 compounds,[6−8] and most convincingly by ^2H NMR line shape analyses of the compound 18C6-$d_4 \cdot 2CH_2(CN)_2$, Buchanan, Ratcliffe, and co-workers[9] have shown that 18C6 experiences large-amplitude motions in its solid complexes. These large-amplitude "merry-go-round" motions are fast (10^5-10^6 jumps s^{-1} at room temperature)[9] and are characterized by a one-sixth rotation followed by an up−down flip. The corresponding onset temperature for these 18C6 motions and their thermal barriers are roughly 200 K and 30−50 kJ mol^{-1}, respectively, depending on the nature of the 18C6 complex. Furthermore, in an independent study of the temperature evolution of the nuclear spin−lattice relaxation of ^{23}Na and ^{123}Cs in the sodide sandwich $[(18C6)_2Cs]^+[Na]^-$, Dye and co-workers also found behavior consistent with an active "merry-go-round" motion of the 18C6 chelates.[10] The corresponding onset temperature is again roughly 200 K, and the thermal barrier is ca. 31 kJ mol^{-1}. Similar solid state motions have now been found in 12C4, 15C5, and 21C7 by NMR methods.[11]

Better understanding of these motions would certainly shed more light on the versatility of 18C6 in cation transport,[12] phase transfer,[13] and modeling of natural and artificial ionophores.[14] Whereas detection and characterization of these solid state motions by NMR methods have been successful, corroborative evidence derived from other techniques is scanty. Besides one

[†] University of the West Indies.
[‡] Louisiana State University.
[§] Department of Chemical Engineering, Tulane University.
[||] Department of Chemistry, Tulane University.
[⊗] Abstract published in *Advance ACS Abstracts,* October 15, 1997.

(1) Fender, N. S.; Finegan, S. A.; Miller, D.; Mitchell, M.; Kahwa, I. A.; Fronczek, F. R. *Inorg. Chem.* **1994**, *33*, 4002.
(2) Kahwa, I. A.; Miller, D.; Mitchell, M.; Fronczek, F. R. *Acta Crystallogr.* **1993**, C*49*, 320.
(3) Kahwa, I. A.; Miller, D.; Mitchell, M.; Fronczek, F. R.; Goodrich, R. G.; Williams, D. J.; O'Mahoney, C. A.; Slawin, A. M. Z.; Ley, S. V.; Groombridge, C. J. *Inorg. Chem.* **1992**, *31*, 3963.
(4) Fairman, R. A.; Gallimore, W. A.; Spence, K. V. N.; Kahwa, I. A. *Inorg. Chem.* **1994**, *33*, 823.
(5) Miyakawa, T.; Dexter, D. L. *Phys. Rev.* **1970**, *B1*, 2961.
(6) Buchanan, G. W.; Morat, C.; Ratcliffe, C. I.; Ripmeester, J. A. *J. Chem. Soc., Chem. Commun.* **1989**, 1306.
(7) Buchanan, G. W.; Kirby, R. A.; Ripmeester, J. A.; Ratcliffe, C. I. *Tetrahedron Lett.* **1987**, *28*, 4783.
(8) Watson, K. A.; Fortier, S.; Murchie, M. P.; Bovenkamp, J. N.; Rodrigue, A.; Buchanan, G. W.; Ratcliffe, C. I. *Can. J. Chem.* **1990**, *68*, 1202.
(9) Ratcliffe, C. I.; Ripmeester, J. A.; Buchanan, G. W.; Denike, J. K. *J. Am. Chem. Soc.* **1992**, *114*, 3294.
(10) Wagner, M. J.; McMills, L. E. H.; Ellaboudy, A. S.; Elgin, J. L.; Dye, J. L.; Edwards, P. P.; Pyper, N. C. *J. Phys. Chem.* **1992**, *96*, 9656.
(11) Ratcliffe, C. I.; Buchanan, G. W.; Denike, J. K. *J. Am. Chem. Soc.* **1995**, *117*, 2900.
(12) Lockhart, J. C. *J. Chem. Soc., Dalton Trans.* **1988**, 1293.
(13) Roeske, R. W.; Gessellchen, P. D. *Tetrahedron Lett.* **1976**, *38*, 3369.
(14) Hilgenfeld, R.; Saenger, W. *Top. Curr. Chem.* **1982**, *101*, 1.

S0020-1669(96)00175-9 CCC: $14.00

Table 1. Numerical Assignments and Properties of Complexes **1**−**13**

				anal., %					
no.	compound	color	yield, %	Br/Cl	C	H	N	density, g cm^{-3}	18C6 orientation
1	$[(Rb18C6)_4MnBr_4][TlBr_4]_2$[a]	tan	92	33.72	21.39	3.62		2.03	
M1	$[(Rb18C6)_4MnBr_4][TlBr_4]_2$[a] molten and annealed	tan							
2	$[(K18C6)_4MnBr_4][TlBr_4]_2$[a]	pale yellow	79	33.99	23.25	4.03		1.89	A
M2	$[(K18C6)_4MnBr_4][TlBr_4]_2$[a] molten and annealed	bright yellow							
3	$[(K18C6)_4ZnBr_4][TlBr_4]_2$[a]	pale yellow	92					1.95	A
4	$[(K18C6)_4MnCl_4][TlCl_4]_2$[a]	colorless	83	16.16	28.78	4.93		1.63	
5	$[(Tl18C6)_4CuBr_4][TlBr_4]_2$[b] 295 K	black	24					2.49	B
6	$[(Tl18C6)_4CuBr_4][TlBr_4]_2$[b] 115 K	black							A
7	$[(Tl18C6)_4MnCl_4][TlCl_4]_2$[b]	very pale yellow	97					2.04	B
8	$[(Tl18C6)_4CuCl_4][TlCl_4]_2$[c]	dark brown	70	15.20	20.77	3.44		2.05	B
9	$[(Tl18C6)_4CuCl_4][TlCl_4]_2 \cdot 0.25H_2O$[c]	dark brown						2.05	A
10	$[(Rb_{1-x}K_x18C6)_4MnBr_4][TlBr_4]_2$[a]	yellow-orange	85−97					1.90−2.02	
M10	$[(Rb_{1-x}K_x18C6)_4MnBr_4][TlBr_4]_2$[a] molten and annealed	yellow-orange							
11	$[(Ba18C6\gamma)_4MnBr_4][TlBr_4]_2$ (γ = Br/OH)[a]	gold	53	34.45	17.34	3.20		2.29	
12	$[(NH_418C6)_4MnBr_4][TlBr_4]_2$[a]	yellow	91		25.37	5.06	2.04	1.77	
13	$[(NH_418C6)_4MnCl_4][TlCl_4]_2$[a]	colorless	55		29.85	5.88	2.68	1.55	

[a] This work. [b] Reference 1. [c] Reference 3.

powder X-ray study revealing 15C5 solid state motion[15] and two differential scanning calorimetric characterizations of the up−down two-site CH_2 flip motion of 12C4[11] and carboxybenzo-24C8,[16] no other type of evidence for such crown ether motions has been reported, to our knowledge.

For the $[(A18C6)_4MnX_4][TlX_4]_2 \cdot nH_2O$ complexes, such large-amplitude conformational changes in the 18C6 chelate can be expected to generate transient static or dynamic crystal defects which may couple to $MnCl_4^{2-}$ electronic states and quench the manganese emission; but any other type of defects independent of the crown ether motion could achieve the same results. On the other hand, water in $[(Tl18C6)_4CuCl_4][TlCl_4]_2 \cdot 0.25H_2O$ is found[3] in the concave faces of 18C6. It is therefore reasonable to expect that large-amplitude "merry-go-round" 18C6 motions could either induce a fluctuating noncentrosymmetric crystal field at the $MnCl_4^{2-}$ center or enable the emission quenching water molecules to diffuse close to the $MnCl_4^{2-}$ species. Both events can enhance $MnCl_4^{2-}$-to-$MnCl_4^{2-}$ and $MnCl_4^{2-}$-to-H_2O energy transfer probabilities. Thus studying energy transport dynamics in $[(A18C6)_4MnX_4][TlX_4]_2 \cdot nH_2O$ crystals not only is important in its own right but is also a potentially good source of vital information about 18C6 solid state motions.

For these reasons, we sought to study the luminescence characteristics of the bromide complexes $[(A18C6)_4MnBr_4][TlBr_4]_2 \cdot nH_2O$. It was hoped that the greater polarizability of the Br^- anions and the higher quantum yield of $MnBr_4^{2-}$ emission compared to that of $MnCl_4^{2-}$ [17] would make the $MnBr_4^{2-}$ ions more sensitive luminescent probes for thermalized solid state 18C6 dynamics in these compounds. The luminescence decay rate of $MnBr_4^{2-}$ is known to be sensitive to phase changes such as fusion.[18]

Herein we report the preparation, structure, and unusual luminescence behavior of the supramolecular complexes $[(A18C6)_4MBr_4][TlBr_4]_2 \cdot nH_2O$ (A = Rb, M = Mn (**1**); A = K, M = Mn (**2**); A = K, M = Zn (**3**)).

Experimental Section

Materials. Potassium bromide was of Spectrosol quality from BDH; rubidium bromide was prepared by neutralization of 99.99% pure rubidium carbonate from Aldrich; 18C6 was of 98% purity from Aldrich; thallium tribromide was obtained by reacting 99.99% pure thallium(III) oxide from Aldrich with concentrated hydrobromic acid; manganese, cobalt, nickel, copper, and zinc dibromides ($MBr_2 \cdot nH_2O$) were of AnalaR quality from BDH.

Syntheses. Complexes **1**−**3** (Table 1) were obtained by slowly evaporating a 2:1 (volume/volume) ethanol/butanol solution containing a stoichiometric mixture of ABr (1 mmol), 18C6 (1 mmol), $MBr_2 \cdot nH_2O$ (0.25 mmol), and $TlBr_3$ (0.5 mmol). This general procedure was also used to prepare $[(K18C6)_4MnCl_4][TlCl_4]_2$ (**4**), which was obtained as colorless crystals of poorly defined morphology. Successful synthesis of $[(K18C6)_4MBr_4][TlBr_4]_2$ (M = Co, Ni, Cu, Zn) was inferred from crystal morphology and density measurements (floatation technique using bromoform and chloroform) which fell in the range 1.91−1.95 g cm^{-3}. Structural similarity to $[(Tl18C6)_4CuBr_4][TlBr_4]_2$ and their chloro analogues[1−3] was established by comparison of powder X-ray diffraction spectra.

Analyses. Analyses of carbon, hydrogen, and bromine were performed by MEDAC, Uxbridge, U.K., while potassium and manganese were determined by atomic absorption spectroscopy using a Perkin-Elmer model 2380 instrument at λ = 766.5 and 279.5 nm, respectively.

Laser Raman Spectra. Single-crystal laser Raman spectra were obtained using a Coherent Innova argon ion laser (λ = 514 nm) and plasma tube. Emission and scattered light were collected by a Jobin Yvon U 1000 spectrophotometer. The photomultiplier tube and thermal cooler were from Products for Research. The data were analyzed by a Dell 210 personal computer.

Cross Polarization Magic Angle Spinning Studies. The Bruker ACE 200 MHZ NMR spectrometer used to record solid state ^{13}C spectra was described previously.[19] The acquisition parameters used were as follows: ^{13}C frequency 50.325 Hz, decoupler power 80 W, contact time 2 ms, recycle time 2 s.

Luminescence Spectra and Lifetime Measurements. The UWI luminescence lifetime measurement setup[4] and variable-temperature equipment[20] used to study **1** and the setup and helium refrigerator at

(15) Doeff, S.; Tsai, K.-L.; Dye, J. L. *Inorg. Chem.* **1991**, *30*, 849.
(16) Buchanan, G. W.; Moghimi, A.; Ratcliffe, C. I. *Can. J. Chem.* **1996**, *74*, 1437.
(17) Wrighton, M.; Ginley, D. *Chem. Phys.* **1974**, *4*, 295.
(18) Presser, N.; Ratner, M. A.; Sundheim, B. R. *Chem. Phys.* **1978**, *31*, 281.
(19) Barrett, D. M. Y.; Kahwa, I. A.; Mague, J. T.; McPherson, G. L. *J. Org. Chem.* **1995**, *60*, 5946.
(20) Fairman, R. A.; Spence, K. V. N.; Kahwa, I. A. *Rev. Sci. Instrum.* **1994**, *65*, 503.

Table 2. Crystallographic Data for **2** and **3**

	2	**3**
empirical formula	$Br_{12}C_{48}H_{96}K_4MnO_{24}Tl_2$	$Br_{12}C_{48}H_{96}K_4O_{24}Tl_2Zn$
fw	2636.3	2646.7
temp, K	296	297
crystal system	cubic	cubic
space group	*F*23 (No. 196)	*F*23 (No. 196)
lattice constants		
a, Å	20.986(7)	20.9682(7)
V, Å^3	9241.8(3)	9219.0(3)
Z	4	4
d_{calc}, g/mL	1.89	1.91
d_{meas}, g/mL	1.91	1.95
F(000)	5036	5056
abs coeff (μ), cm^{-1}	90.20	91.77
scan mode	$\omega-2\theta$	$\omega-2\theta$
θ limits, deg	1−32 (octant)	1−30 (octant)
no. of unique reflcns	1443	1216
no. of obsd reflcns	672	668
no. of variables	71	71
R^a	0.062	0.036
$R_w{}^b$	0.037	0.039
resid dens, e Å^{-3}	4.55	1.09

^{a} $R = \sum||F_o| - |F_c||/\Sigma|F_o|$. ^{b} $R_w = (\sum w(|F_o| - |F_c|)^2/\sum wF_o^2)^{1/2}$.

Tulane University[21] used to study **2** were described earlier. A Questak Series 2000 Vβ excimer laser (λ = 309 nm) pumping a coumarin 460 laser dye from Kodak was used to measure lifetimes of **2**. Excitation of the $MnBr_4^{2-}$ chromophore was in all cases at 479 nm. Luminescence and excitation spectra were recorded on a Perkin-Elmer LS-5 fluorescence spectrophotometer.

Powder X-ray Diffraction. Powder X-ray diffraction spectra were obtained using a Siemens model D5000 diffractometer.

Crystal Structure Determinations. The essential experimental conditions and resulting crystallographic data are given in Table 2. Data reduction in both cases included corrections for background and Lorentz and polarization effects, and absorption corrections were based on ψ scans. Both the manganese and zinc complexes crystallize in the cubic *F*23 space group and are isomorphous with the structure of $[(Tl18C6)_4CuBr_4][TlBr_4]_2$ at 115 K; thus coordinates from the $[(Tl18C6)_4CuBr_4][TlBr_4]_2$ complex were used as starting trial refinement models. Non-hydrogen atoms were refined anisotropically by full-matrix least-squares procedures using Enraf-Nonius MolEN programs.[22] The hydrogen atoms were idealized, assigned isotropic thermal parameters ($B = 1.3B_{eq}$ of attached C), and allowed to ride on the parent carbon atoms. The absolute structure of **3** was established by the *R* factor ratio test, with the inversion-related structure yielding $R = 0.059$, $R_w = 0.064$; refinement of the inversion-related structure for **2** was inconclusive, possibly due to the lower quality of the crystals or inversion twinning.

Results and Discussion

Syntheses and Crystal Structures. Successful preparation of compounds **1**−**4** is indicated by elemental analyses (Table 1). A comparison of room-temperature powder X-ray diffraction patterns of **1**−**3** (Figure 1) with those of their cubic *F*23 chloro analogues, $[(A18C6)_4MCl_4][TlCl_4]_2$ (Figure 1, ref 4), reveals considerable similarities and supports the conclusion that the bromide and chloride salts are isomorphous.[1−3] As with the chloride series, members of the $[(Rb18C6)_4MBr_4][TlBr_4]_2$ series with M = Mn, Co, Ni, Cu, and Zn are also readily synthesized; observed similarities in crystal morphology and densities (g cm^{-3}), i.e. 1.91 (Co), 1.93 (Ni), 1.92 (Cu), and 1.95 (Zn), are consistent with their isomorphism. The Raman spectra of $[(A18C6)_4MBr_4][TlBr_4]_2$ (A = Rb, K; M = Mn, Zn) are similar and are dominated by bands due to the more polarizable T_d $TlBr_4^-$ species occurring at ca. 182 cm^{-1} (ν_1 (symmetrical stretching)) ca. 198 cm^{-1} (ν_3 (asymmetrical stretching)), ca. 52 cm^{-1} (ν_2 (bending)), and ca. 65 cm^{-1} (ν_4 (bending)); bands due to T_d MBr_4^{2-} appear as weak features at ca. 172 cm^{-1} (ν_1 (symmetrical stretching)), ca. 208 cm^{-1} (ν_3 (asymmetrical stretching)), and ca. 91 cm^{-1} (ν_4 (bending)).

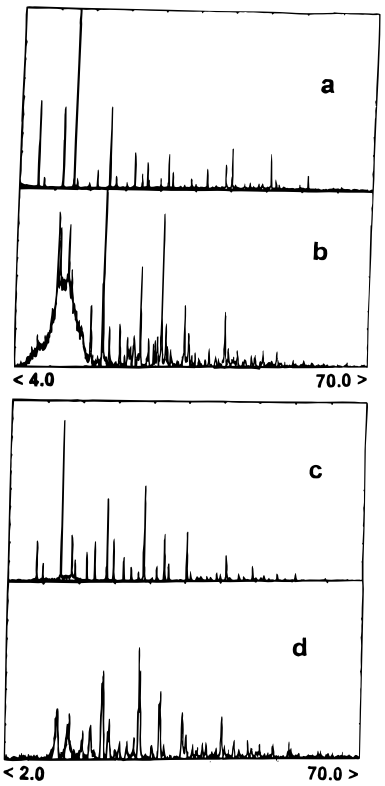

Figure 1. The essentially similar powder X-ray diffraction spectra of (a) **2**, (b) the corresponding thermally treated sample (see text), **M2**, (c) **1** and (d) **M1**.

Table 3. Atomic Positions and Equivalent Isotropic Thermal Parameters for **2** (Esd's in Parentheses)

atom	*x*	*y*	*z*	B_{eq},^{a} Å^2
K(1)	0.3571(1)	1 − *x*	*x*	5.14(3)
Tl(2)	0	0	0	4.11(3)
Tl(3)	1/4	1/4	1/4	3.77(3)
Mn	3/4	1/4	1/4	6.3(2)
Br(1)	0.81586(8)	1 − *x*	1 − *x*	13.24(3)
Br(2)	0.07014(6)	*x*	*x*	6.29(2)
Br(3)	0.17971(6)	*x*	*x*	5.89(2)
O(1)	0.4734(3)	0.6533(3)	0.2900(3)	5.3(2)
O(4)	0.4071(3)	0.5430(3)	0.2742(3)	5.8(2)
C(2)	0.4986(6)	0.6018(5)	0.2548(7)	6.5(3)
C(3)	0.4457(6)	0.5725(6)	0.2255(6)	7.8(4)
C(5)	0.4954(6)	0.7435(6)	0.3530(5)	6.8(3)
C(6)	0.5237(4)	0.6879(5)	0.3158(5)	4.9(3)

^{a} $B_{eq} = (8\pi^2/3)\sum_i\sum_j U_{ij}a^*_i a^*_j a_i \cdot a_j$.

Since there were difficulties with the preparation of **4** (vide supra) and the luminescence characteristics of the bromide analogue **2** were very unusual (vide infra), it was important to obtain a detailed crystal structure of the potassium complexes. Atomic coordinates are given in Tables 3 and 4 for **2** and **3**, respectively, while interbond distances and angles are shown in Tables 5 and 6. One of the four $K18C6^+$ complex cations which are coordinated to the four faces of the MBr_4^{2-} tetrahedron is shown in Figure 2 for **3**. The $K18C6^+$ is in the "sunrise" mode as is typical for members of this family of cubic *F*23 complexes;[1−3] the position of the K^+ ions above the least-

(21) Matthew, K. D.; Bailey-Folkes, S. A.; Kahwa, I. A.; McPherson, G. L.; O'Mahoney, C. A.; Ley, S. V.; Williams, D. J.; Groombridge, C. J.; O'Connor, C. J. *J. Phys. Chem.* **1992**, *96*, 7021.
(22) Fair, C. K. *MolEN: An Interactive Structure Solution Procedure*; Enraf-Nonius: Delft, The Netherlands, 1990.

Table 4. Atomic Positions and Equivalent Isotropic Thermal Parameters for **3** (Esd's in Parentheses)

atom	*x*	*y*	*z*	B_{eq},[a] Å^2
K(1)	0.3555(1)	$1 - x$	*x*	4.67(3)
Tl(2)	0	0	0	3.92(3)
Tl(3)	$^1/_4$	$^1/_4$	$^1/_4$	3.66(3)
Zn	$^3/_4$	$^1/_4$	$^1/_4$	2.86(7)
Br(1)	0.81461(6)	$1 - x$	$1 - x$	7.66(2)
Br(2)	0.07040(6)	*x*	*x*	5.78(1)
Br(3)	0.17962(6)	*x*	*x*	5.63(1)
O(1)	0.4755(3)	0.6538(3)	0.2912(4)	4.8(2)
O(4)	0.4060(3)	0.5411(4)	0.2780(3)	5.1(2)
C(2)	0.4987(8)	0.5998(5)	0.2559(6)	6.0(3)
C(3)	0.4430(6)	0.5661(6)	0.2269(5)	5.6(3)
C(5)	0.4950(6)	0.7440(5)	0.3544(5)	5.5(3)
C(6)	0.5246(5)	0.6887(7)	0.3224(6)	5.3(3)

[a] $B_{eq} = (8\pi^2/3)\sum_i\sum_j U_{ij}a^*_i a^*_j a_i \cdot a_j$.

Table 5. Interatomic Distances for **2** and **3** (Esd's in Parentheses)

	distances, Å	
bond × multiplicity	M= Zn	M = Mn
M−Br(1) × 4	2.3466(8)	2.3939(9)
Tl(2)−Br(2) × 4	2.5568(9)	2.5494(7)
Tl(3)−Br(3) × 4	2.5561(7)	2.5547(7)
K(1)−M × 1	3.832(2)	3.894(2)
K(1)−Br(1) × 3	3.7677(7)	3.8315(7)
K(1)−O(1) × 3	2.861(7)	2.825(6)
K(1)−O(4) × 3	2.909(7)	2.981(7)
O(1)−C(2) × 3	1.44(1)	1.41(1)
O(1)−C(6) × 3	1.42(1)	1.39(1)
O(4)−C(3) × 3	1.42(1)	1.44(1)
O(4)−C(5) × 3	1.40(1)	1.44(1)
C(2)−C(3) × 3	1.49(1)	1.41(2)
C(5)−C(6) × 3	1.48(1)	1.52(2)

Table 6. Bond Angles for **2** and **3** (Esd's in Parentheses)

	angles, deg	
bond	M= Zn	M = Mn
K(1)−M−Br(1)	70.53(2)	70.53(2)
K(1)−M−Br(1)	180	180
K(1)−Br(1)−K(1)	112.28(5)	112.17(4)
K(1)−Br(1)−M	73.51(3)	73.38(4)
M−K(1)−Br(1)	35.96(2)	36.09(2)
M−K(1)−O(1)	101.3(1)	99.5(1)
M−K(1)−O(4)	108.5(1)	106.1(2)
Br(1)−K(1)−Br(1)	61.13(4)	61.35(4)
Br(1)−K(1)−O(1)	74.84(1)	72.8(1)
Br(1)−K(1)−O(1)	91.6(1)	90.5(1)
Br(1)−K(1)−O(1)	135.2(2)	133.4(1)
Br(1)−K(1)−O(4)	73.9(1)	71.3(1)
Br(1)−K(1)−O(4)	131.4(2)	128.8(2)
Br(1)−K(1)−O(4)	112.8(1)	111.6(1)
O(1)−K(1)−O(1)	116.2(2)	117.3(2)
O(1)−K(1)−O(4)	57.9(2)	56.5(2)
O(1)−K(1)−O(4)	150.2(2)	154.2(2)
O(1)−K(1)−O(4)	58.5(2)	60.9(2)
O(4)−K(1)−O(4)	110.4(2)	112.6(2)
C(2)−O(1)−C(6)	113.4(9)	108(1)
C(3)−O(4)−C(5)	111.9(8)	120(1)
O(1)−C(2)−C(3)	109(1)	106(1)
O(4)−C(5)−C(6)	109(1)	115(1)
O(1)−C(6)−C(5)	108(1)	108(1)

squares plane of the six crown ether oxygen atoms (Figure 2) is 0.639(2) and 0.742(2) Å for **2** and **3**, respectively.

Although the potassium bromide complexes **2** and **3** are generally isomorphous with their thallium chloro and bromo analogues characterized previously,[1−3] close examination reveals some subtle contrasts. For example, the structures of the anhydrous $[(Tl18C6)_4CuBr_4][TlBr_4]_2$ complex (**5**) at 295 and 115 K are both cubic *F*23. But the orientation of the 18C6 chelate in the cryogenic structure (orientation A) differs from

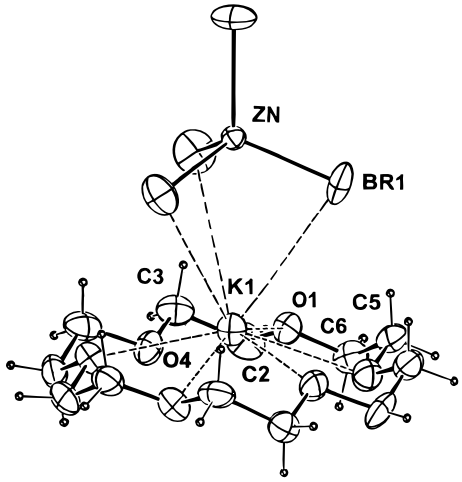

Figure 2. Facial binding of one of the four $K18C6^+$ ions to the $ZnBr_4^{2-}$ tetrahedron in **3**, showing typical sunrise conformation.[1−3]

that found in the room-temperature structure (orientation B) by a ca. 30° rotation with respect to the C_3 axes of the $[(Tl18C6)_4CuBr_4]^{2+}$ moiety (Figures 1 and 2, ref 1). This is the most compelling evidence for 18C6 motion in its solid state complexes. Whereas the strong Jahn−Teller character of the $CuBr_4^{2-}$ anion might have some energetic influence on the relative stability of orientations A and B, structural evidence from complexes of non-Jahn−Teller ions which are isomorphous with $[(Tl18C6)_4CuBr_4][TlBr_4]_2$ reveals that other factors are more important. Specifically, orientation B is found in the room-temperature structures of the anhydrous salts of **5**, **7**, and **8**, while orientation A is seen in the cryogenic structure of the anhydrous copper bromide complex **6** and the room-temperature structure of the hydrated copper chloride complex **9**.[1−3] In sharp contrast to the behavior of other anhydrous cubic *F*23 salts, the room-temperature structures of the anhydrous potassium manganese and zinc bromide complexes **2** and **3** feature 18C6 in orientation A. These 18C6 orientational differences are not detectable by powder X-ray diffraction methods as the diffraction patterns of **2** and **3** (Figure 1) are similar to those of complexes featuring 18C6 in orientation B (Figure 1a, ref 4). Although direct evidence for the factors influencing these 18C6 orientational preferences is lacking, orientation A seems to occur in compounds in which $MX_4^{2-}\cdots$18C6 repulsive interactions are expected to be greatest. For example, the presence of H_2O in the concave faces of 18C6 in **9** may lead to closer repulsive $CH_2\cdots CuCl_4^{2-}$ contacts when the crown oxygens bind to H_2O by hydrogen bonding. Similarly, repulsive $CH_2\cdots MnBr_4^{2-}$ contacts are expected to be significant in **2** and **3**, where the small K^+ ion sinks deeper into the 18C6 cavity (vide supra) than found in analogous thallium compounds such as **7**. It is thus possible that orientation A is adopted by **2** and **3** to minimize repulsive interactions.

Cross Polarization Magic Angle Spinning (CP MAS). No conclusion can be made from the above structural data as to whether 18C6 orientations A and B correspond to different locked 18C6 conformations or fast dynamic X-ray diffraction invisible averages. Locked and dynamic solid state 18C6 conformations can be distinguished by CP MAS ^{13}C NMR if there is sufficient difference in crown carbon torsional environments.[7] For both **2** and **3**, the carbon atom torsional environments are essentially similar. Each 18C6 carbon atom in **3** is involved in one quasi gauche conformation on the C−C bond with torsional angles 66(1)° for C_2-C_3 and 70(1)° for C_5-C_6

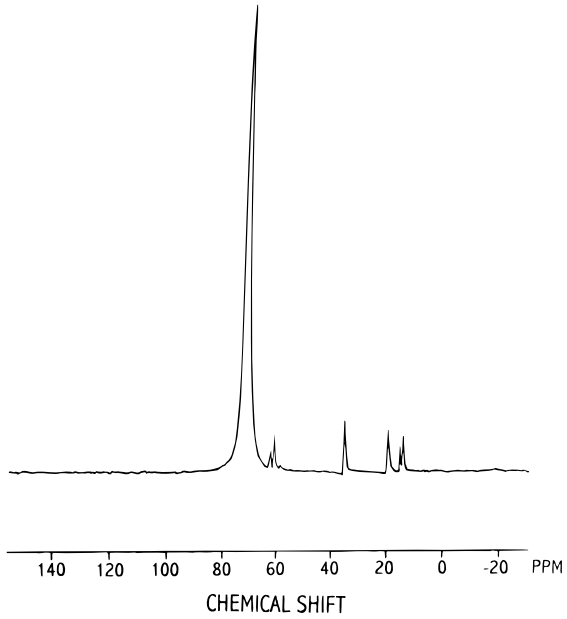

Figure 3. CP-MAS ^{13}C spectrum of **3** in the CH_2 region at 295 K.

and three quasi trans conformations on each O−C bond with torsion angles in the range 174−179(1)°. The corresponding parameters for **2** are −68(1), 64(1), and 174−180(1)°. However, the D_{3d} conformation of the $K18C6^+$ units requires that there be two distinct sets of carbon atoms: those which are up and therefore more shielded by the $ZnBr_4^{2-}$ ions and those which are down, i.e. further away from the $ZnBr_4^{2-}$ ions and thus less shielded. If these differences are significant and the 18C6 conformations are locked, at least a pair of ^{13}C resonances should appear in the room-temperature ^{13}C CP MAS spectrum as is true for the [K18C6]NCS complex.[7] The CP MAS ^{13}C NMR spectrum of **3** at 295 K (Figure 3) exhibits a single, broad, featureless peak in the 60−70 ppm range. This result suggests that the 18C6 chelate is conformationally dynamic at room temperature, and the equivalence of the up and down carbon atoms would then be consistent with the "merry-go-round" 18C6 motion proposed by Ratcliffe, Ripmeester, Buchanan, and Denike.[9]

Luminescence Spectral Characteristics. Since the proposed "merry-go-round" motion is known to be temperature dependent and the $MnBr_4^{2-}$ luminescence decay dynamics are well-known for their sensitivity to thermalized solid state effects,[15] we sought to study the temperature evolution of the luminescence characteristics of $[(A18C6)_4MnBr_4][TlBr_4]_2$ complexes. It was hoped that, in the event of a transition from a locked to a dynamic 18C6 conformational mode, the resulting inhomogeneity of the paramagnetic centers would lead to a noticeable increase in quenching rates of $[(A18C6)_4MnBr_4]^{2+}$ emission. Since the structure of **2** was solved, it was a good starting point for our luminescence studies.

Quite unusually, **2** emits very weakly at 77 K with a strange $\lambda_{max} \approx 575$ nm (Figure 4) and luminescence at room temperature is unobservable. Because of this strange behavior, we turned to the luminescence of the rubidium compound, $[(Rb18C6)_4MnBr_4][TlBr_4]_2$ (**1**), for comparison. The behavior of **2** contrasts sharply with that of **1**; in typical T_d $MnBr_4^{2-}$ ($^4T_1(^4G)$) character, **1** emits strongly at 77 K with $\lambda_{max} \approx 535$ nm (Figure 4). The room-temperature emission is weak but observable. The excitation spectra of the emission from both manganese(II) complexes, **1** and **2** monitored at 535 and 610 nm, are similar (Figure 4) and feature absorptions largely typical

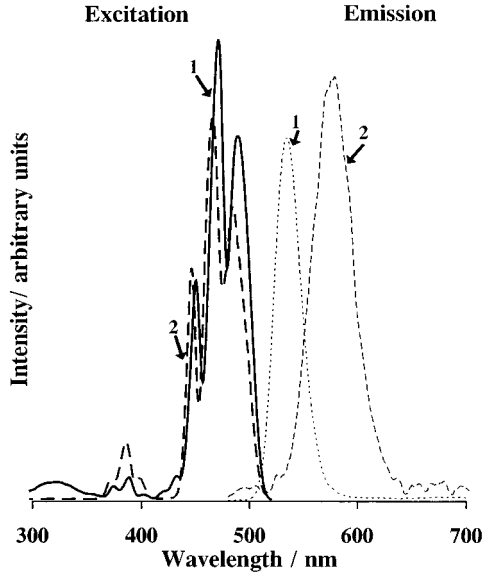

Figure 4. Excitation spectra ($\lambda_{em} = 540$ nm) of **1** and **2** and the unusual emission spectrum ($\lambda_{exc} = 360$ nm) of **2** compared to the normal T_d $MnBr_4^{2-}$ emission shown by **1** at 77 K.

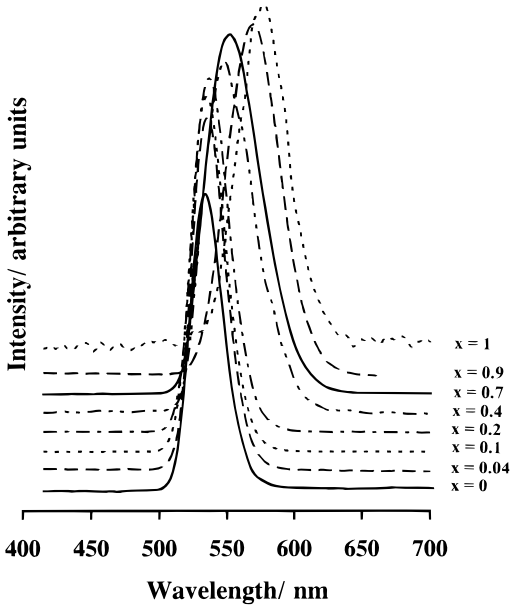

Figure 5. Emission spectra ($\lambda_{exc} = 372$ nm; 77 K) of the mixed potassium/rubidium complexes, **10**, showing a gradual shift from T_d $MnBr_4^{2-}$ emission ($\lambda_{em} \approx 525$ nm) toward dominant trap emission ($\lambda_{em} \approx 575$ nm) with increasing concentration of potassium.

of T_d $MnBr_4^{2-}$ species.[14,15,23,24] It seems that the unusual luminescence spectrum of **2** is due to a trap which is a good quencher of $MnBr_4^{2-}$ emission. In an attempt to remove or minimize these traps, we repeatedly recrystallized **2**; subsequent analyses, however, did not show significant changes in the luminescence λ_{max} or spectral profile. We then studied the behavior of a series of mixed $[(Rb_{1-x}K_x18C6)_4MnBr_4][TlBr_4]_2$ (**10**) complexes which were crystallized from solution in order to determine the evolution of the luminescence behavior with increasing potassium concentration. The luminescence spectral evolution (Figure 5) of **10** with increasing x shows the contribution of the species emitting at 575 nm to be increasing with the concentration of potassium ions and eventually

(23) de Lucas, M. M.; Rodriguez, F. *J. Phys.: Condens. Matter* **1989**, *11*, 4251.
(24) Cotton, F. A.; Goodgame, D. M. L.; Goodgame, M. J. *J. Am. Chem. Soc.* **1962**, *84*, 167.

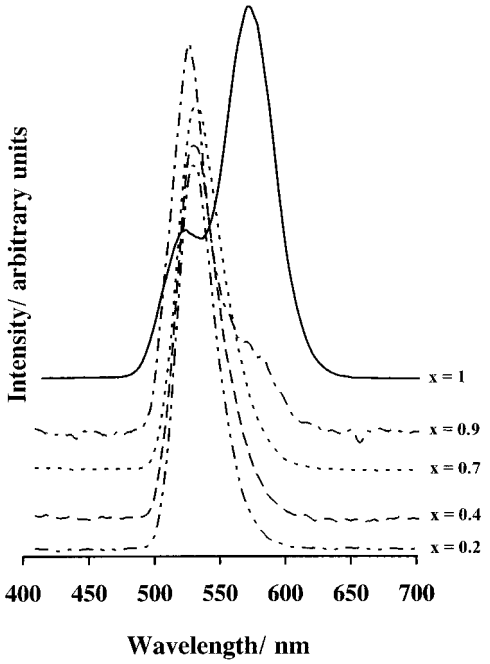

Figure 6. Emission spectra ($\lambda_{exc} = 372$ nm; 77 K) of thermally treated mixed potassium/rubidium complexes, **M10** ($x = 0.2-1$), showing distinctly T_d $MnBr_4^{2-}$ ($\lambda_{em} \approx 525$ nm) and trap ($\lambda_{em} \approx 575$ nm) emission.

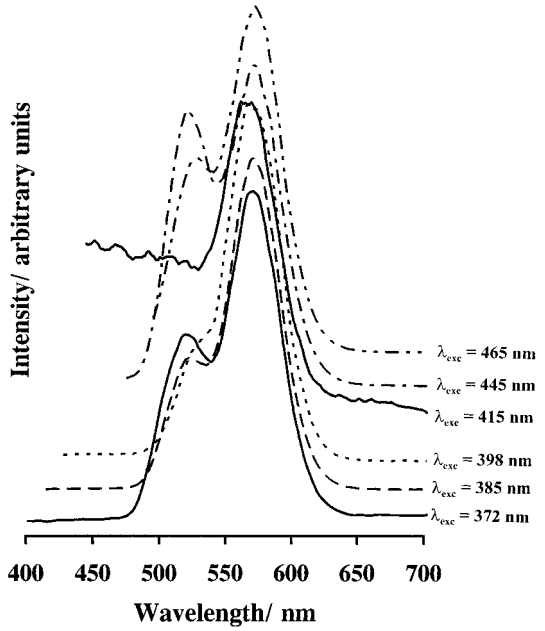

Figure 7. Emission spectra ($\lambda_{exc} = 372$ nm; 77 K) of thermally treated potassium complex, **M2**, showing the effect of excitation at varying energies.

becoming dominant for the pure potassium complex ($x = 1$) (**2**). We thus attribute the unusual emission at $\lambda_{max} \approx 575$ nm to crystal defects which are associated with the introduction of K^+ ions. In a further attempt at minimizing the population of the crystal defects in **1**, **2**, and **10**, these samples were fused and annealed; generally, all samples exhibit similar melting points in the range 170−220 °C. To complete the comparative characterization, the complexes $[(Rb18C6)_4MBr_4][TlBr_4]_2$ and $[(K18C6)_4MBr_4][TlBr_4]_2$ (M = Co, Ni, Cu, Zn) were prepared and found to melt in the same range. All samples were heated until they completely melted and were then annealed at 169 °C for 24 h; the resulting compounds are **M1**, **M2**, and **M10** (Table 1).

Comparison of the powder X-ray diffraction spectra of the thermally treated **M1** and **M2** and their untreated counterparts, **1** and **2** (Figure 1), shows that thermal treatment does not change the basic cubic *F*23 structure for both **1** and **2**. But the peaks for **M2** are broadened, showing decreased crystallinity compared to those of **M1**. The luminescence spectra and lifetimes of **M1** and **1** are similar, indicating that the heat treatment did not alter the local and extended electronic environments of the $MnBr_4^{2-}$ ions in this compound. However, in sharp contrast to the behavior of **M1**, thermally treated potassium-containing samples **M2** and **M10** exhibit a most spectacular display of the luminescence behavior of the crystal defects (Figure 6). The emission spectra of **M10**, especially that of the pure potassium sample, **M2**, exhibit two distinct bands; a normal T_d $MnBr_4^{2-}$ ($^4T_1(^4G)$) peak at $\lambda_{max} \approx 525$ nm is now resolved from the unusual defect emission at $\lambda_{max} \approx 570$ nm (Figure 6, $x = 1$). Crystals of $[(K18C6)_4MnBr_4][TlBr_4]_2$ (**M2**) obtained from the fusion-annealing process appear to have either a less efficient quenching regime for $MnBr_4^{2-}$ emission or poorly emitting traps. Either of these reasons or both could lead to the relatively stronger and better resolved $MnBr_4^{2-}$ emission of **M2**. Further, we have varied the energy of the excitation light and obtained both the 525 and 570 nm emission bands except for $\lambda_{exc} \approx 415$ nm, for which only the 570 nm emission is observed (Figure 7). From these results we conclude that the unusual emitter in **2** ($\lambda_{em} \approx 575$ nm), **11**, **M10**, and particularly **M2** ($\lambda_{em} \approx 575$ nm) is a crystal defect site associated with the introduction of the small K^+ ions (ionic radius = 1.38 Å compared to 1.49 Å for Rb^+)[25] into the cubic *F*23 lattice. This crystal defect is a good quencher for $MnBr_4^{2-}$ emission and might have a prominent absorption at ca. 415 nm although this is not evident from the excitation spectrum dominated by $MnBr_4^{2-}$ absorptions. An Mn^{2+} crystal defect site is a particularly good possibility, and the absorption in the neighborhood of 415 nm would in this case correspond to (^4E, ^4A) ← $^6A_1$ absorptions which are almost independent of the crystal field strength.

Luminescence Decay Dynamics. The luminescence spectra discussed above show conclusively that emission of $[(A18C6)_4MnBr_4]^{2+}$ species in **1**, **2**, **M2**, and **M10** is influenced by temperature-dependent quenching processes. There are two types of $[(A18C6)_4MnBr_4]^{2+}$ emission quenching regimes: (1) the quenching process which is devoid of visible acceptor emission, *e.g.* in **1**, and (2) the quenching process which results in acceptor emission at ca. 570−575 nm, *e.g.* in **2**, **11**, **M2**, and **M10**. Since the acceptor emission is not observed from these compounds at room temperature, it must itself be quenched.

However, the difference in the nature of quenchers of $[(A18C6)_4MnBr_4]^{2+}$ emission in **1** and **2** as well as acceptors of trap emission in **2** and **M2** are still obscure. It was therefore interesting to study the temperature evolution of the luminescence decay rates of **1** and **2**, which can shed more light on energy transport dynamics in these crystals and the behavior of the active emission quenchers.

$[(Rb18C6)_4MnBr_4][TlBr_4]_2$ (1). The luminescence decay behavior of **1** was studied in the temperature range 77−295 K with emission set at $\lambda_{em} = 535$ nm and excitation at 479 nm. At $T < 180$ K, the luminescence decay curves are exponential for over 3.5 lifetimes (Figure 8a) and the corresponding temperature-independent decay rate k_{s1} is ca. 2.8×10^3 s^{-1}, which is similar to the normal spontaneous decay rate for $MnBr_4^{2-}$ emission.[14] But at $T > 180$ K, temperature-dependent luminescence decay behavior prevails. For $180 < T \leq 210$ K, the decay curves are exponential (Figure 8b), while nonexponential behavior is found for $210 < T \leq 240$ K (Figure 8c).

(25) Shannon, R. D.; Prewitt, C. T. *Acta Crystallogr.* **1969**, *B25*, 925.

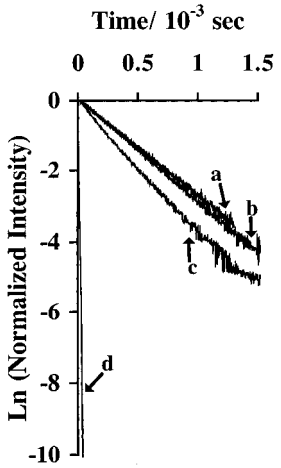

Figure 8. Representative logarithmic plots of the luminescence decay of **1** in the four temperature ranges, showing difference in rates and exponentiality with temperature (observation temperature $= T_o$): (a) $T < 180$ K, $T_o = 77$ K; (b) $180 < T < 210$ K, $T_o = 192$ K; (c) $210 < T < 240$ K, $T_o = 223$ K; (d) $T > 240$ K, $T_o = 298$ K. Normalized intensity = observed intensity/intensity at $t = 0$.

With $T > 240$ K, the temperature-dependent decay curves are again exponential (Figure 8d). Therefore, in the $180 < T \leq 210$ K and $T > 240$ K temperature ranges, the energy transport behavior of **1** is in the dynamic regime,[26] while an intermediate regime[27] dominates in the range $210 < T \leq 240$ K. For **1**, setting the observed luminescence decay rate $= k_{o1}$ and the spontaneous decay rate $= k_{s1}$, the trapping rate $= k_{t1}$ becomes (Table 7)

$$k_{t1} = k_{o1} - k_{s1} \quad (1)$$

The thermal barrier to the emission-quenching process can now be calculated from the corresponding Arrhenius plot ($\ln k_{t1}$ vs $1/T$) (Figure 9). For the dynamic regimes $180 < T \leq 210$ and $T > 240$ K, the thermal barriers are 8 ± 0.4 and 14 ± 0.1 kJ mol^{-1}, respectively. For the intermediate region $210 < T \leq 240$ K, the rate of the fast-decaying component, which is more representative of trapping events, may be approximated by fitting the decay curves to double-exponential models. When these rates are used as the input k_{o1} in eq 1, the k_{t1} rates so obtained (Table 7) yield a thermal barrier of 26 ± 0.2 kJ mol^{-1} for the process responsible for the faster quenching events in the temperature range $210 < T \leq 240$ K.

$[(K18C6)_4MnBr_4][TlBr_4]_2$ (2). The luminescence decay behavior of **2** was studied in the temperature range 18−300 K with emission set at 511 nm for the normal T_d $MnBr_4^{2-}$ emission and 610 nm for the unusual crystal defect emission; excitation was maintained at 479 nm. Consistent with the terminology used for **1**, the observed decay rate is designated as k_{o2G} for the green emission at 511 nm and k_{02R} for the trap emission monitored at 610 nm; the corresponding spontaneous decay rates are k_{s2G} and k_{s2R} and the trapping rates are k_{t2G} and k_{t2R} (Table 7).

In sharp contrast to the behavior of **1**, the decay curves of **2** monitored at 511 nm are temperature independent and exponential for at least 3.5 lifetimes for only $T < 23$ K. The corresponding k_{s2G} of ca. 2.8×10^3 s^{-1} is similar to the normal spontaneous luminescence decay rate of $MnBr_4^{2-}$ species.[14] For $T > 23$ K, the intensity of the emission at 511 nm falls, the decay curves deviate from exponentiality, and at about 110 K, luminescence becomes too weak to measure free of the accompanying trap emission. Rough estimates of the thermal barrier, $E_{A2G} \approx 4 \pm 0.2$ kJ mol^{-1}, to quenching of the 511 nm emission were made using trapping rates k_{t2G} derived from eq 2 with k_{o2G} values from exponential approximations to the early time decay curves.

$$k_{t2G} = k_{o2G} - k_{s2G} \quad (2)$$

Table 7. Temperature Evolution of the Observed Luminescence Decay Rates (k_o) and Corresponding Trapping Rates (k_t) for **1** ($\lambda_{em} = 511$ nm) and **2** ($\lambda_{em} = 610$ nm)

	1		**2**	
T, K	k_o, s^{-1}	k_t, s^{-1} [a]	k_o, s^{-1}	k_t, s^{-1} [a]
18			2200	
23			2080	
52			2050	
66				
77	2770			
80			2940	740
91			4860	2660
100			10050	7850
123			67570	65370
133			98040	95840
144			196080	193880
154			359710	357510
163			500000	497800
171	2770			
173			675680	673480
181			1094010	1091810
183	2830	60		
192	3040	270	1459850	1457650
201			1915710	1913510
202	3180	400		
208	3180[b]	400		
	11200[c]	8500		
210			2242150	2239950
211	11000[c]	8200		
213	12700[c]	9900		
220	40000[c]	37200		
230	34500[c]	31700		
243	66700	63900		
250	71400	68700		
260	100000	97200		
273	142900	140100		
298	217400	214600		

[a] Rounded off; $k_t = k_o - 2770$ s^{-1} for **1** and $k_o - 2200$ s^{-1} for **2**; 2770 and 2200 are the temperature-independent decay rates. [b] Marginally satisfactory fit to exponential kinetics. [c] k_o = fast decaying component approximated by double-exponential fits.

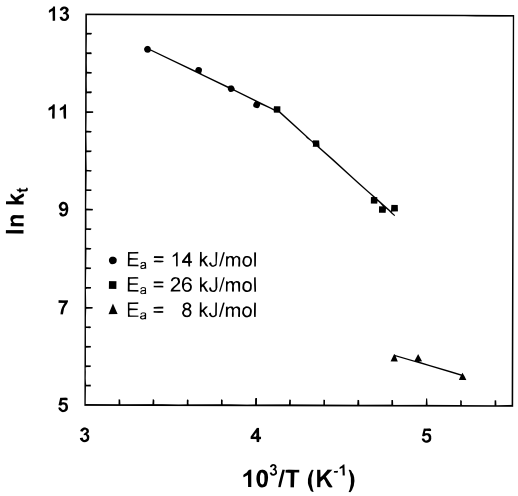

Figure 9. Temperature evolution of the luminescence ($\lambda_{em} = 535$ nm) decay rates of **1** (Arrhenius plot) in the temperature range 180−300 K. The datum of 220 K is omitted.

(26) Yokota, M.; Tanimoto, O. *J. Phys. Soc. Jpn.* **1967**, *22*, 779.
(27) Huber, D. L. *Phys. Rev.* **1979**, *B20*, 2307.

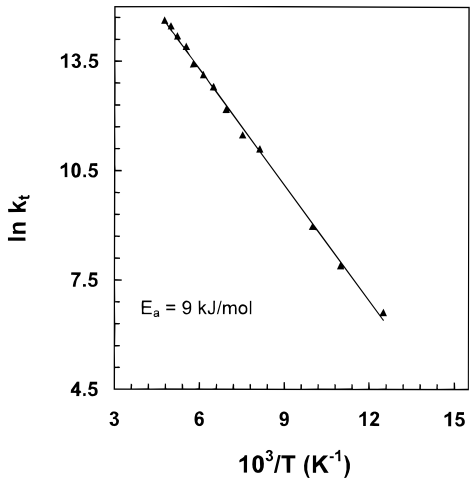

Figure 10. Temperature evolution of the luminescence (λ_{em} = 610 nm) decay rates of **2** (Arrhenius plot) in the temperature range 77−210 K.

The orange trap emission monitored at 610 nm yields exponential and temperature-independent decay curves in the range 18−52 K. The corresponding spontaneous decay rate is $k_{s2R} \approx 2.0 \times 10^3$ s^{-1} and shows an excitation build-up of ca. 8.6×10^3 s^{-1}, which is of a similar order of magnitude as the decay rate of the $MnBr_4^{2-}$ emission. With $T > 52$ K, the trap luminescence is quenched but the decay curves remain exponential up to 110 K. The decay curves are then nonexponential for $110 < T \leq 130$ K but do resume exponential character from 130 up to 210 K, after which the emission is too weak to measure. For regions corresponding to dynamic regimes, namely $110 < T \leq 130$ K and $130 < T \leq 210$ K, the decay curves were fitted to single exponentials to obtain k_{o2R}. For $110 < T \leq 130$ K, double-exponential approximations were used to obtained the average decay rate of the fast-decaying component which was taken to be k_{o2R}. The thermal barrier, E_{A2R}, to quenching of the trap emission is from the relationship

$$k_{t2R} = k_{o2R} - k_{s2R} \tag{3}$$

and the corresponding Arrhenius plot (Figure 10) gives $E_{A2R} \approx 9 \pm 0.01$ kJ mol^{-1}, which is remarkably similar to the thermal barrier of $MnBr_4^{2-}$ quenching in **1** in the range $180 < T \leq 210$ K.

In an attempt to determine the generality of the temperature-dependent characteristics found in complexes **1** and **2**, we prepared other cubic *F*23 compounds, viz. $[(Ba18C6\gamma)_4MnBr_4][TlBr_4]_2$ (**11**) and $[(NH_418C6)_4MnX_4][TlX_4]_2$ (X = Br, **12**; X = Cl, **13**), and studied their luminescence behavior. The Ba^{2+} ion, the radius of which is ca. 1.36 Å for coordination number 6, is similar to that of K^+, while the tetrahedral NH_4^+ has an ionic radius of ca. 1.48[28] (*cf.* Rb^+ and Tl^+). It was hoped that luminescence behavior which is influenced largely by A^+ ions could be clarified in a comparative study of the behavior of **1**, **2**, and **10**−**13**. Weak emission was found for the barium bromide complex (λ_{max} = 525 nm with a shoulder at ≈570 nm). The ammonium bromide complex **12** exhibited a slightly quenched but normal luminescence with $\lambda_{max} \approx 512$ nm and decay rate 3.1×10^3 s^{-1} at 77 K; at room temperature, emission vanishes. The green emission from **13** peaks at $\lambda_{max} \approx 520$ nm (Figure 11) and is quenched. The decay curves monitored at 510, 540, and 600 nm are nonexponential at room temperature, and the corresponding decay rates, which

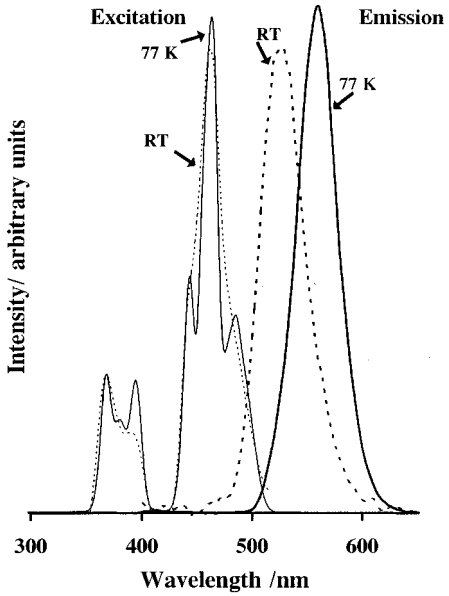

Figure 11. Excitation and emission (λ_{exc} = 365 nm) spectra of **13** showing unusual ($\lambda_{max} \approx 558$ nm) emission at 77 K compared to normal T_d $MnBr_4^{2-}$ ($\lambda_{max} \approx 521$ nm) emission at room temperature.

are ca. 10^4 s^{-1} for the early part and 4.5×10^3 s^{-1} for the tail, are unusually high for $MnCl_4^{2-}$. Most interestingly, at 77 K, emission from **13** is unusually yellow and the overall λ_{max} of the emission envelope is ca. 560 nm (Figure 11). The 77 K decay curves monitored at 510 nm are exponential, and the corresponding decay rate is ca. 2.6×10^2 s^{-1}, but those monitored at 558 and 585 nm are marginally exponential over 4 lifetimes and the decay rates are ca. 5.7×10^2 s^{-1} for the early part and 2.5×10^2 s^{-1} for the tail. The detailed luminescence behavior of the ammonium complexes is under study to determine the nature of the emitting species in **12** and **13**.

General Remarks

The luminescence characteristics of **1**, **2**, **4**, **5**, and **10**−**13** show that the energy transport processes in these cubic *F*23 supramolecular systems feature two luminescence-quenching regimes: one in which the quencher is itself a good emitter and another in which it is not. There is, however, no conclusive evidence with which to derive, unequivocally, the nature of the luminescence traps in these systems. But since there is no evidence for phases other than cubic *F*23 in the single crystal and powder X-ray diffraction studies, the conclusion that traps of the $[(A18C6)_4MnBr_4]^{2+}$ emission in **1** and **2** are crystal defects is very reasonable. These defects might as well be Mn^{2+} species in effective coordination environments of non-T_d or O_h overall crystal field symmetry. We have pursued this possibility synthetically and found new manganese compounds with Mn^{2+} in eight-fold (D_{4d}) coordination, viz. $[Mn(12C4)_2][MnBr_4]_2$-$[(CH_3)_4N]_2$ (**14**), and seven-fold coordination, viz. $[Mn15C5\text{-}(D_2O)_2][MnBr_4]\cdot D_2O$ (**15**), which emit rather strongly in the region 550−610 nm.[29] The $[Mn(12C4)_2]^{2+}$ species in **14** is an efficient quencher of $MnBr_4^{2-}$ emission and features an emission at ca. 550 nm which decays exponentially at only 29 s^{-1} at 77 K.

There is no straightforward explanation for the temperature evolution of the decay rates of the luminescence of **1** and **2**. What is unambiguous, however, is that, with $T < 210$ K, the

(28) Atkins, P. W. *Quanta*, 2nd ed.; Oxford University Press: New York, 1991.

(29) Reid, H. O. N.; Kahwa, I. A.; White, A. J. P.; Williams, D. J. Unpublished work.

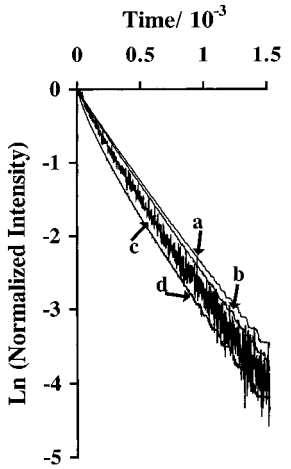

Figure 12. Logarithmic plots of 77 K emission decay curves (λ_{exc} = 479 nm). **2**: (a) λ_{em} = 610 nm; (b) λ_{em} = 530 nm. **M2**: (c) λ_{em} = 610 nm; (d) λ_{em} = 530 nm. Normalized intensity = observed intensity/ intensity at $t = 0$.

thermal barrier to $MnBr_4^{2-}$ luminescence quenching in **1** and the emitting trap in **2** is about 9 kJ mol^{-1}. We attribute this thermal barrier to the energy needed to maintain efficient energy migration on the $MnBr_4^{2-}$ sublattice. That is, the vibronic energy required for the Stokes shifted exciton-donating $MnBr_4^{2-}$ $^4T_1(^4G)$ state to come to resonance with the acceptor $^4T_1(^4G)$ state of the neighboring $MnBr_4^{2-}$ ion. From Figure 4, the donor emission is at ca. 18 900 cm^{-1}, while the origin of the $^4T_1(^4G)$ state is at ca. 19 760 cm^{-1}; the difference between the two is ca. 1060 cm^{-1}, or 12.7 kJ mol^{-1}, which is close to the observed 9 kJ mol^{-1} thermal barrier.

The best model for **1** and **2** and their derivatives is one in which a few traps are present and energy migration on the $MnBr_4^{2-}$ sublattice is efficient. In this case, the regular $^4T_1$-(^4G) $MnBr_4^{2-}$ excitation in **1** and **2** should migrate throughout the crystal until it encounters crystal defects where it is trapped. Some of the traps may be luminescent as in the cases of **2**, **M2**, **10**, and **M10**. However, this trap emission could be quenched by back energy transfer to the T_d $MnBr_4^{2-}$ ions. This possibility is plausible in view of the near thermal equilibration of the green and orange emission decay rates of **2** and **M2** in the neighborhood of 77 K (Figure 12) and similar luminescence quenching thermal barriers of 8 and 9 kJ mol^{-1} for **1** and **2**, respectively, at $T < 210$ K. The 14 kJ mol^{-1} thermal barrier for $T > 240$ K in **1** is also close to the energy required to bridge the $^4T_1(^4G)$ states of donor and acceptor T_d $MnBr_4^{2-}$ ions. It is therefore attributed to the thermal barrier for energy migration on the $MnBr_4^{2-}$ sublattice. There is no significant energy migration in **1** at $T < 180$ K since introduction of Cu^{2+} traps in $[(Rb18C6)_4(MnBr_4)_{1-x}(CuBr_4)_x][TlBr_4]_2$ leads to nonexponential decay behavior at 77 K, with x being as little as 0.01. For both **1** and **2**, significant increase in luminescence quenching activity is observed at $T > 200$ K, and for **1**, the largest increases are in the range $210 < T \leq 240$ K. It is possible that these rapid increases in luminescence decay rate correspond to the onset of large-amplitude solid state 18C6 "merry -go-round" motions which are inferable from the CP MAS ^{13}C spectrum (Figure 3) and are commonly found in 18C6 compounds.[6] The thermal barrier of 26 kJ mol^{-1} found for **1** is close to the value of $E_a \approx$ 33 kJ mol^{-1} predicted by the Waugh−Fedin approximation[30] for hindered rotation in solids

$$E_a \text{ (kJ mol}^{-1}) \approx 0.155T_c \quad (4)$$

where T_c = transition temperature (ca. 210 K for **1**).

The Waugh−Fedin approximation is valid if $10 \leq E_a/RT \leq 25$; with E_a = 26 kJ mol^{-1} and $T = 180-240$ K, the region of interest for **1** is $13 < E_a/RT < 19$, which is well within the validity requirements. This thermal barrier of 26 kJ mol^{-1} is similar to the values of 30−50 found by Buchanan, Ratcliffe, et al.[6] for several 18C6 compounds and ca. 30 kJ mol^{-1} for the sodide $[Cs(18C6)_2]^+[Na]^-$ reported by Dye et al.,[10] who studied the solid state 18C6 motion by a variety of NMR techniques. The "merry-go-round" 18C6 motion described by Buchanan, Ratcliffe, et al.[9] requires two independent motions: rotation and up−down flips to maintain the D_{3d} symmetry of the 18C6. Either one of these motions could impose a thermal barrier to the "merry-go-round" motion. Since the observed thermal barrier of 26 kJ mol^{-1} is close to the value of 30 kJ mol^{-1} predicted for torsion angle deformation in 18C6,[31] the up−down flip may be the rate-determining step for the 18C6 motion in **1**. For the cubic $F23$ chlorides $[(A18C6)_4MnCl_4][TlCl_4]_2$, a higher thermal barrier of ca. 50 kJ mol^{-1} is found to correspond to rapid increases in the trapping rate of $[(A18C6)_4MnBr_4]^{2+}$ by crystal water molecules.[4] Further studies covering compounds with ammonium ions in A sites and substituted 18C6 chelates, such as $18C6CH_2OH$, have been undertaken to shed more light on the factors influencing the energy transport processes in the cubic $F23$ supramolecular system and their implications for the 18C6 solid state motions.

Acknowledgment. We thank the Chemistry Department, UWI, for a demonstratorship and a departmental award to N.S.F. and the Board of Postgraduate Studies and Research and Publications Committees of the UWI, The Royal Society of Chemistry (London), The Third World Academy of Sciences, and The National Science Foundation for financial support and the European Development Fund for a grant with which the NMR spectrometer was acquired. We also thank Dr. Richard A. Fairman and Mr. Kirk V. N. Spence (UWI), who wrote the computer programs for luminescence experiments done at UWI, the Jamaica Bauxite Institute for use of the powder X-ray diffractometer, and the Forensic Laboratory (Jamaica) for loan of the luminescence spectrophotometer.

Supporting Information Available: Tables of H atom coordinates and anisotropic displacement parameters for **2** and **3** and figures showing the partial molecular structure with atom labeling and the stereoscopic packing of **2** (7 pages). Ordering information is given on any current masthead page.

IC9601753

(30) Waugh, J. S., Fedin, É. I. *Sov. Phys. Solid State* **1963**, *4*, 1633.
(31) Wippf, G.; Weiner, P.; Kollman, P. *J. Am. Chem. Soc.* **1982**, *104*, 3249.